Research Square

Preprints are preliminary reports that have not undergone peer review.
They should not be considered conclusive, used to inform clinical practice,
or referenced by the media as validated information.

From rain to radiance - Dominant climate drivers of tropical carbon flux interannual variability depend on local hydroclimate

Shuang Ma
California Institute of Technology
Junjie Liu
junjie.liu@jpl.nasa.gov
California Institute of Technology
A. Anthony Bloom
California Institute of Technology
Russell Doughty
University of Oklahoma
Paul A. Levine
California Institute of Technology
T. Eren Bilir
California Institute of Technology
Alexander Norton
The University of Melbourne
Renato K. Braghiere
California Institute of Technology
John R. Worden
California Institute of Technology
David S. Schimel
California Institute of Technology

Article

Keywords: Tropics, interannual-variation, carbon cycle, climate drivers, El Niño, La Niña

Posted Date: June 9th, 2026

DOI: https://doi.org/10.21203/rs.3.rs-9596159/v1

License: This work is licensed under a Creative Commons Attribution 4.0 International License.
Read Full License

Additional Declarations: No competing interests reported.

From rain to radiance - Dominant climate drivers of tropical carbon flux interannual variability depend on local hydroclimate

Shuang Ma[1,2,*], Junjie Liu[1,3@], A. Anthony Bloom[1], Russell Doughty[4], Paul A. Levine[1,3], T. Eren Bilir[1], Alexander Norton[5], Renato K. Braghiere[3,1], John R. Worden[1], David S. Schimel[1]

1. Jet Propulsion Laboratory, California Institute of Technology, Pasadena, United States
2. Joint Institute for Regional Earth System Science and Engineering, University of California, Los Angeles, Los Angeles, United States
3. Division of Geological and Planetary Sciences, California Institute of Technology, Pasadena, United States
4. University of Oklahoma, Atmospheric and Geographic Sciences, OK, United States
5. The University of Melbourne, School of Geography, Melbourne, Australia

*Now at The University of Oklahoma foundation, Inc.

@ Corresponding author email: junjie.liu@jpl.nasa.gov

© 2026. All rights reserved.

Key points

1. The dominant climate drivers for GPP interannual variability (IAV) shift with mean local hydroclimate
2. The dominant climate drivers for NEE_{IAV} more closely mirror ER than GPP
3. The dominant climate drivers for carbon fluxes IAV are climate-state-dependent across both space and time

Abstract

Tropical land carbon fluxes dominate the interannual variability (IAV) of atmospheric CO_2 growth, yet the climate controls and underlying mechanisms remain debated. We use a Bayesian data-assimilation framework that integrates multiple satellite-based carbon and water observations to quantify the relative contributions of key climate drivers to tropical land carbon-flux IAV at the grid-cell scale and their dependence on local hydroclimate. Along a gradient from very wet to very dry climates, the contributions of temperature, radiation, and vapor pressure deficit systematically decline, while the contribution of precipitation increases. In dry and very dry regions (<1500mm/yr), precipitation explains more than 40% of the IAV in gross primary production (GPP), ecosystem respiration (ER), and net ecosystem exchange (NEE), but only ~0–20% in very wet regions (>2500mm/yr). Conversely, radiation contributes up to ~40% of GPP_{IAV} and ~20% of ER_{IAV} and NEE_{IAV} under very wet conditions. These hydroclimate dependencies also vary seasonally and during climate extremes. We further show that climate contributions are governed primarily by carbon-flux sensitivities rather than by the magnitude of climate anomalies. Our results imply that dominant climate controls on tropical carbon-flux IAV will shift with future climate, underscoring the need to represent climate-dependent sensitivities in carbon-cycle projections.

Keywords

Tropics, interannual-variation, carbon cycle, climate drivers, El Niño, La Niña

Teaser

Mean hydroclimate states determine the dominant climate drivers of interannual variability of tropical carbon exchange

1. Introduction

The sensitivity of tropical net land carbon fluxes to interannual climate variability is shown to be closely linked to how the tropical land carbon pools respond to future climate change[1]. Yet, identifying the dominant climatic controls on tropical carbon-flux interannual variability (IAV) remains challenging, owing to the region's climatic heterogeneity, ecological complexity, and sparse observations. Earlier studies found a substantial correlation between tropical land temperature variability and the IAV of tropical net ecosystem exchange (NEE) [1–5]. In recent years, an increasing number of studies have shown a tight coupling between water availability and tropical net carbon flux variability [6,7]. Interestingly, some studies find that these relationships are not stationary: the sensitivity of tropical net carbon fluxes to both temperature and water availability has intensified in recent decades, implying that carbon-climate sensitivity evolve with the mean climate itself [8,9].

However, most existing evidence is derived from pan-tropical analyses that rely on atmospheric CO_2 growth rate as a proxy for the IAV of tropical net land carbon fluxes, implicitly assuming homogeneous climate controls across the tropics. This assumption is challenged by regional studies, which reveal pronounced spatial contrasts in the dominant climatic drivers of carbon flux variability. For instance, radiation plays a dominant role in controlling photosynthetic variability in the wet Amazon [10–14], while variations in water availability critically shape the carbon flux variability in semi-arid and sub-tropical ecosystems [15,16]. Jung et al.[17] also demonstrate that inferred climate controls depend strongly on spatial scales: temperature dominates globally integrated NEE_{IAV}, whereas water availability governs the IAV of gross primary productivity (GPP), ecosystem respiration (ER), and NEE at latitudinal scales.

These sporadic regional and global studies collectively show that the dominant climate drivers for tropical carbon flux IAV vary in both space and time. However, a comprehensive analysis of the spatiotemporal variations of the contributions of different climate drivers to tropical carbon flux IAV and how these variations relate to mean climate states remains lacking. Quantifying these spatiotemporal variations and their dependency on mean climate is essential for improving predictions of tropical carbon flux IAV under future climate change, particularly given projected non-uniform climate changes across the tropics: widespread drying in tropical South America, increasing rainfall in parts of tropical Africa (IPCC AR6), and the ongoing increases in temperatures, vapor pressure deficit (VPD)[18], dry season length[19], and severe drought events[20].

To fill this knowledge gap, we systematically investigate the dominant climate drivers for tropical carbon fluxes IAV with a Bayesian data-assimilation modeling framework CARDAMOM[21] (Methods). We

examine (1) how the climate drivers for tropical carbon flux IAV, including NEE and its component fluxes, vary across space and time at local and regional scales; and (2) the relationships between spatiotemporal variations of dominant climate driver contributions to IAV and mean climate states. By integrating a suite of satellite observations to constrain variables such as NEE, GPP, and total water storage (TWS) in a process-based land model, CARDAMOM can better represent processes controlling carbon flux variability and the water-carbon cycle coupling. Especially, with constraints on both GPP and NEE, the system can better represent ecosystem respiration, which has much larger uncertainty than photosynthetic process[22]. Additionally, the modeling framework allows us to mechanistically quantify the contributions of multiple climate factors to tropical carbon flux IAV and to understand how the dominant climate factors vary across space and time, thereby enhancing the granularity of climate controls on tropical carbon flux IAV. We examine NEE and its component fluxes (GPP, ER) to understand the compensating/aggregating effect of climate drivers – such as temperature, precipitation, VPD, radiation, and their interactions.

RESULTS

Dominant climate drivers differ for GPP_{IAV}, ER_{IAV}, and NEE_{IAV} and shift with local hydroclimate regimes

The seasonal and IAV of observational data at each grid cell are captured by the Data Assimilation Linked Ecosystem Carbon model (DALEC) at both the local and continental scales (Figure S1-S7). At the regional scale, CARDAMOM simulations are strongly correlated with assimilated net biosphere exchange (NBE), GPP, and TWS ($r > 0.5$), with all correlations statistically significant at the 99% confidence level ($p<0.01$), indicating that the data-constrained CARDAMOM framework effectively captures observed carbon-climate coupling. Detailed results on data-model integration are in the Supplement (Text S1). To evaluate the relative importance of precipitation (P), VPD (V), shortwave radiation (R), temperature (T), and their interactions (I), on carbon (C) flux variability, we replace one climatic driver at a time with their climatological means in the perturbed model runs and calculate their carbon fluxes differences (dC) from the control model runs (scenarios are listed in Table S1). The carbon response index (K) is calculated as the time series mean of the absolute value of dC. The K index essentially quantifies the importance of each climate driver on carbon flux variabilities, capturing both its concurrent and lagged effect (Methods).

The dominant climate factors for NEE_{IAV} and its component fluxes are heterogeneous (Figure 1). Radiation dominates GPP_{IAV} in the moist rainforests in the Amazon and part of Congo, while VPD drives the variability of GPP_{IAV} in the seasonally moist rainforests on both continents (Figure 1A and Figure S8). In southeast tropical South America, as well as the north- and south-east of tropical Africa, where the lowest Mean Annual Precipitations (MAP) occurs (Figure 2A), GPP_{IAV} is driven by precipitation. In regions near the Andes, temperature emerges as the dominant driver of GPP_{IAV} (Figure S8). A similar but weaker pattern is found for ER, mainly due to the strong dominance of precipitation over heterotrophic respiration (Rh, Figure S9). The dominant climate factor for NEE_{IAV} is the net outcome of ER_{IAV} and GPP_{IAV} (Figure 1C), but its spatial distribution mirrors ER_{IAV} more than GPP_{IAV} (Figure 1C and Figure S8).

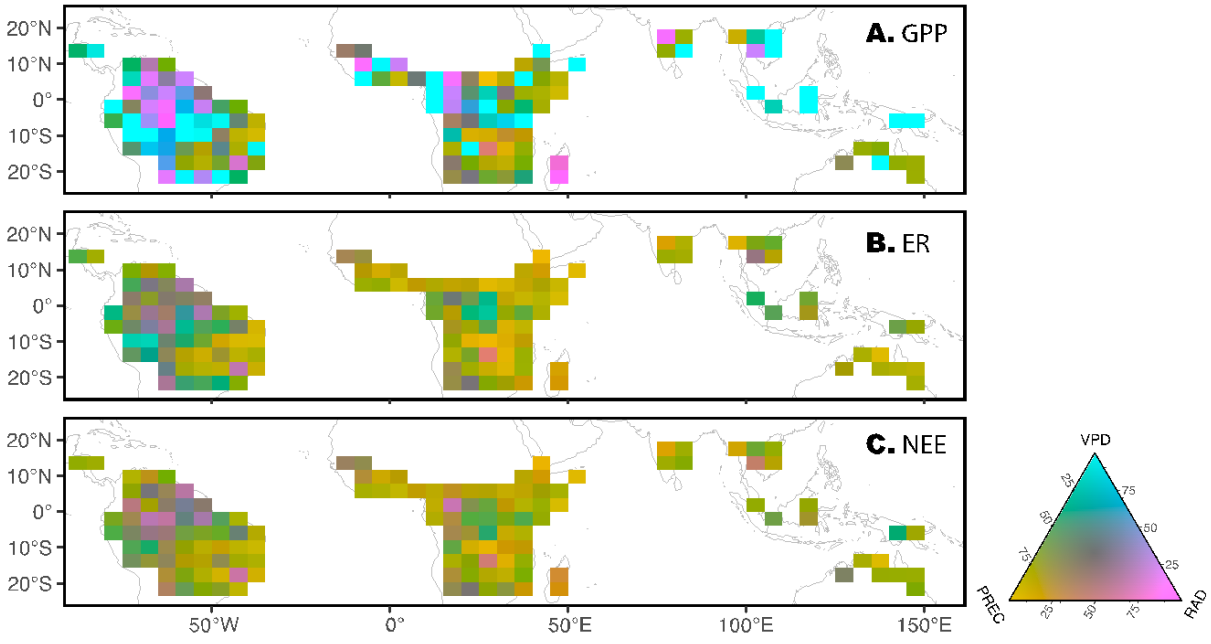


Figure 1. Maps showing the dominant climate factors for net carbon exchange (NEE) (C) and its component fluxes GPP (A) and ER (B) during 2010-2021. The three largest climate factors for carbon fluxes IAV, precipitation, VPD, and shortwave radiation, are chosen to calculate their relative importance in these ternary maps.

To understand how the dominant climate factors of C flux IAV shifts in the tropic regions, we calculated correlations between relative contributions of climate factors to C flux IAV and their environmental and biological mean states (mean monthly minimum temperature, mean monthly maximum

125 temperature, total precipitation, VPD, radiation, above- and belowground biomass (ABGB), soil organic C
126 (SOC)) (Figure S10). We find that dominant climate factors for GPP_{IAV} shift with mean precipitation (r=-
127 0.98) and radiation gradient (r=0.87) (Figure S10 A and B) such that the GPP_{IAV} in wetter and drier
128 environments is driven by different factors. Other mean climate states, as well as ABGB and SOC, are to a
129 lesser degree correlated with the relative importance (Figure S10 C-G). A similar shifting of dominant
130 climate drivers is also found for ER_{IAV} and NEE_{IAV}. We use mean annual precipitation in relevant figures
131 and discussions hereafter, to highlight the role of mean hydroclimate state in determining the relative
132 contributions of different climate factors to C fluxes IAV.

133 To further quantify how the contributions of climate factors to C fluxes IAV change with
134 precipitation gradient, we group the tropical grid points into five categories based on their annual mean
135 precipitation (Figure 2a-d). These five categories are: very dry (0-1000 mm/year), dry (1001-1500
136 mm/year), semi-dry (1500-2000 mm/year), wet (2000-2500 mm/year), and very wet (above 2500 mm/year)
137 (Figure 2A). The relative contributions of precipitation to C fluxes IAV decrease while the relative
138 contributions of VPD, radiation, and temperature increase as the mean precipitation becomes higher, which
139 is especially apparent for GPP_{IAV}. The median value of the precipitation contribution to GPP_{IAV} decreases
140 from 42% in the very dry region to nearly 0% in the very wet region. In contrast, the relative contributions
141 of VPD to GPP_{IAV} increase from 21% in the very dry region to over 40% in the wet and very wet regions,
142 while the relative contribution of radiation to GPP_{IAV} rises from 0% in the very dry region to above 10% in
143 the wet and very wet regions (Figure 2b).

144 For both NEE_{IAV} and ER_{IAV}, precipitation remains the dominant factor across almost all climate
145 groups, but its influence weakens as the regions become wetter. Specifically, its contribution to ER_{IAV}
146 declines from around 60% in the very dry region to about 30% in the very wet region, while its contribution
147 to NEE_{IAV} decreases from 50% to 35% (Figure 2 C and D). Simultaneously, the role of radiation, VPD, and
148 temperature becomes more important as the regions become wetter. In the very wet region, the temperature

contributes 30% to ER_{IAV}, slightly higher than precipitation contribution and almost double its contribution in the very dry region.

These climate zones differ in their dominant vegetation types. The very-dry to dry climate zones are characterized by grasslands, croplands, shrublands, and savannas, while wet and very-wet regions are dominated by seasonally moist rainforest and rainforests. The interconnectivity between climate and vegetation types, along with shifts of dominant climate factors driving C fluxes IAV with mean hydroclimate, suggests that the relative contributions of different climate factors may also vary by vegetation types (Figures S11-12). For example, precipitation accounts for about 50% to GPP_{IAV} in grassland where the climate falls in the very-dry category, whereas its contribution to GPP_{IAV} in rainforest, where the MAP falls in the very-wet category, is close to 0% and the radiation contribution is 50%.

However, even within the same vegetation types, the relative contributions of various climate factors differ between tropical Africa and South America. In tropical Africa, precipitation is a more important climate factor in driving C fluxes IAV, while radiation and VPD are more important in tropical South America (Figure 1 and Figure S12). For example, precipitation contributes approximately 50% to GPP_{IAV}, ER_{IAV}, and NEE_{IAV} of semi-arid vegetation in tropical Africa (Figure 1 and Figure S11-S12). In contrast, for the same vegetation type in tropical south America, precipitation only contributes 12%, 25% and 37% to GPP_{IAV}, ER_{IAV}, and NEE_{IAV} respectively, while VPD plays a more significant role, contributing about 25% (Figure 1 and Figure S11-S12). This contrast is largely due to differences in the mean precipitation, which is lower over tropical Africa than over tropical South America, even for the same vegetation type (Figure 2A and Figure S11). These results highlight the critical role of mean hydroclimate rather than vegetation types in shaping the relative contributions of different climate factors to C fluxes IAV across the tropics.

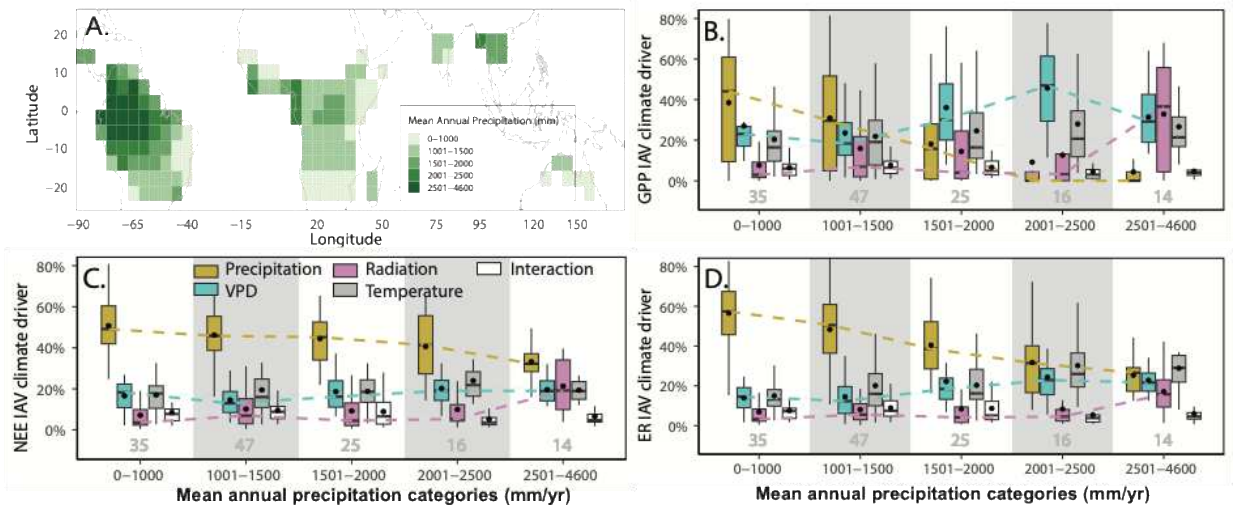


Figure 2. The Mean Annual Precipitation (MAP) determines relative contributions of climate factors to the IAV of GPP, ER, and NEE (2010-2021). Grid-cell data is grouped according to the MAP, which is shown in (A). Boxes and whiskers show relative contributions from each climate factor and their interactive effect to the IAV of GPP (B), ER (D), and NEE (C) at each MAP category. Dark yellow: precipitation; blue: VPD, magenta: radiation; grey: temperature; white: interaction. The gray numbers at the bottom are the number of 4º (latitude) x 5º (longitude) within each MAP category.

Wet and dry seasons affect dominance of climate factors

The previous section demonstrates that the spatial distribution of dominant climate factors is closely linked to the spatial pattern of annual mean precipitation (Figures 1-2). However, precipitation also exhibits pronounced seasonal and interannual variabilities in the tropics. Here and in the following section, we evaluate whether the dominant climate drivers of carbon flux variability depend not only on long-term mean climate but also on the timing of climate variability. Specifically, we examine whether carbon flux anomalies caused by climate anomalies depend not only on where the climate anomalies occur, but also on when they occur. In this section, we compare the dominant climate factors in the dry/wet seasons during 2010-2021. Wet (dry) seasons are defined as consecutive months with precipitation above (below) the climatological annual mean[23].

The general heterogeneous pattern does not change across the annual average, dry seasons, or wet seasons (Figure 1 and Figure 3). However, precipitation becomes less important, and radiation and VPD

become more important for GPP_{IAV}, NEE_{IAV}, and ER_{IAV} during the wet seasons over semi-arid ecosystems, corresponding to the higher precipitation states. Radiation becomes the dominant climate factor for GPP_{IAV} even over the seasonally moist forest in the Amazon, and for NEE_{IAV} and ER_{IAV} over the moist forest in the Amazon during the wet season (Figure 3).

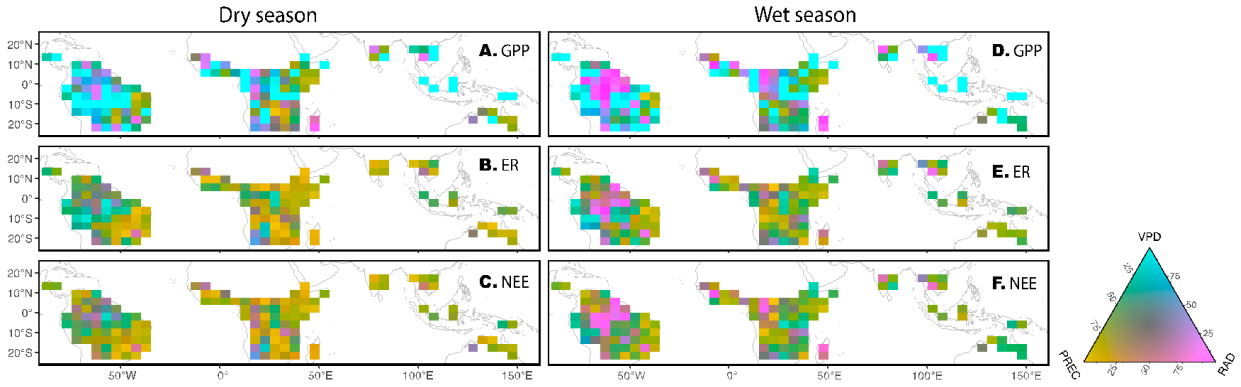


Figure 3. The dominant climate factors for carbon flux IAV depends on seasons. Maps showing the dominant climate factors for GPP (A and D), ER (B and E), and net carbon exchange (C and F) during dry (left column) and wet (right column) seasons of 2010-2021. The three largest climate factors for carbon fluxes IAV, precipitation, VPD, and radiation, are chosen to calculate their relative importance in these ternary maps.

During the dry season, VPD, precipitation or temperature instead of radiation makes the largest contribution to GPP_{IAV}, NEE_{IAV}, and ER_{IAV} in the wet and very-wet pixels (Figures 3). The role of radiation on GPP_{IAV} is less prominent even in the very-wet pixels. The radiation only contributes 20% (Figure S13) to GPP_{IAV} during the dry season in the very-wet pixels, less than the 40% in the annual average (Figure 2) and 70% during the wet season (Figure S13). Over those very-wet pixels, the relative contributions of radiation to NEE_{IAV} also reduce from 23% during the wet season to 10% during the dry season, while the relative contributions of VPD to NEE_{IAV} increase from 13% to 20% (Figure S13). The similar changes also occur over those pixels categorized as wet.

The relative contributions of precipitation to carbon flux IAV are larger during the dry season than during the wet season over all those pixels categorized as dry and semi-dry, while the relative contributions of VPD become stronger during the wet season (Figure 3 and Figure S13). For example, precipitation and

211 VPD contribute 44% and 11% to NEE_{IAv} during the dry season in the dry pixels, while they are 38% and
212 20% respectively during the wet season (Figure S13). Similar magnitude shifts are also observed for ER_{IAv}
213 and GPP_{IAv} over the same pixels. Over the very-dry pixels, the relative contributions of precipitation are
214 similar between the dry season and wet season, but VPD becomes a much more important factor during the
215 wet season (Figure 3, Figure S13). VPD contributes 20% to GPP_{IAv} during the dry season, but 40% during
216 the wet season over those very-dry pixels (Figure S13). This contrast of the dominant climate factors
217 between dry seasons and wet seasons is also found for El Niño vs La Niña (next section).

218 **El Niño and La Niña modify the intensity of dominant climate factors**

219 El Niño and La Niña have the largest impact on the tropical climate interannual variations, with drier climate
220 anomalies during El Niño and wetter climate anomalies during La Niña. The last section shows that the
221 relative contributions of climate factors to C flux IAV depend on which season it happens. In this section,
222 we investigate whether the relative contributions of climate factors to C flux IAV would also depend on
223 whether it is dry climate anomalies – El Niño, or wet climate anomalies – La Niña by quantifying the
224 relative contributions of various climate factors to C flux IAV during the strongest El Niño (drier, May
225 2015-April 2016) and La Niña (wetter, July 2010-December 2011) months within our data-constrained
226 period (2010-2021).

227 The general heterogeneous pattern does not change across the 2010-2021 annual average (Figure
228 1), 2015-2016 El Niño (Figure 4), and 2010-2011 La Niña months (Figure 4). However, we find similar
229 contrasting changes between El Niño and La Niña as between wet and dry seasons. During El Niño, the
230 dominant role of radiation on GPP_{IAV} is less obvious even in the wettest part of the Amazon Forest (mean
231 MAP>2800mm, Figure 4). It changes from a median value of 50% in the annual average to a median value
232 of 37% during the 2015-2016 El Niño. VPD becomes an even more important driver during El Niño for the
233 seasonally moist rainforest in the Amazon and Congo as well as the wetter semi-arid ecosystems and
234 grassland (semi-dry to wet pixels) (Figure S14). For example, over the wet pixels, the median value of VPD

contributions to GPP_{IAV} changes from 47% during the annual average to 58% during 2015-2016 El Niño (Figure S14). The relative importance of precipitation to NEE_{IAV} during 2015-2016 El Niño does not change significantly from the annual average, but the temperature becomes a more important factor, attributing to the increasing contributions of temperature in ER anomaly during that period (Figure S14 and Figure 2).

During the 2010-2011 La Niña, when vegetation is less water stressed due to the larger-than-usual amount of precipitation across the tropics, VPD takes over the dominance of precipitation on GPP_{IAV} in the driest pixels (mean MAP<1000mm), especially over African semi-arid ecosystems and grassland (Figure S14B and Figure 4). During the 2010-2011 La Niña, the mean precipitation over African semi-arid ecosystems and grassland, and Asian/Australian grassland were 14mm, 59mm, and 342mm higher than the climatology precipitation during the same months. As a result, precipitation becomes a less important driver for GPP_{IAV} in the same regions. It changed from a median value of 35% to 10%. Even though the shifting of relative contributions of climate drivers from El Niño to La Niña is broadly consistent with the changes from dry season to wet season, the contrast of relative contributions is much smaller. This is because the climate contrast between El Niño and La Niña is less than the difference between the dry and wet seasons. The contrasting relative contributions of climate drivers to carbon flux IAV between dry and wet seasons and between El Niño vs. La Niña imply that the dependence of dominant climate factors for carbon flux IAV on mean hydroclimate also applies in time.

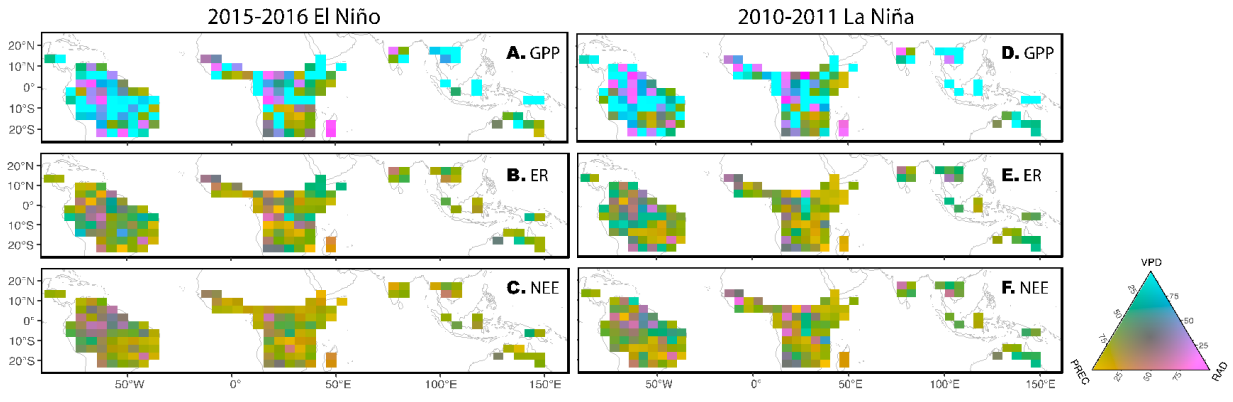


Figure 4. The dominant climate factors for carbon flux IAV depends on whether it is dry or wet climate anomalies. Maps showing the dominant climate factors for GPP (A and D), ER (B and E), and NEE (C and F) during 2015-2016 El Niño (dry climate anomalies) (left column) and 2010-2011 La Niña (wet climate anomalies) (right column). The three largest climate factors for carbon fluxes IAV, precipitation, VPD, and radiation, are chosen to calculate their relative importance in these ternary maps.

Shifts in climate contributions to carbon flux IAV are driven by flux sensitivity rather than climate anomalies

The contribution of any climate driver to C flux IAV is the product of climate anomaly and the sensitivity of carbon flux to that climate anomaly. In this section, we address whether the shifting of the relative contributions of climate drivers to C flux IAV in both space and time is primarily due to changes in the magnitude of climate anomaly or the sensitivity of carbon flux to that climate anomaly.

Figure 5 shows the relative sensitivities of GPP, ER, and NEE to climate anomaly and the magnitude of climate anomalies at each MAP category. The multiplication of the sensitivities of C flux to climate anomaly and climate anomaly itself would be the contribution of that climate driver to the C flux IAV shown in Figure 2. Figure 5D shows that the changes of relative magnitude of climate anomalies across MAP categories are much smaller than the changes of relative sensitivities of C fluxes to those climate anomalies (Figure 5 A-C). Additionally, the gradient of the sensitivities of C fluxes to climate anomalies across MAP categories almost exactly mirror the relative contributions of each climate factor to C flux IAV (Figure 2). This suggests that the shifting of the relative contributions of climate drivers to C flux IAV in space is primarily due to the changes in the sensitivities of carbon flux to climate anomalies, not due to the magnitude of climate anomalies.

For example, radiation anomaly is the weakest in the very-wet pixels compared to elsewhere, whereas the highest GPP sensitivity to radiation is found in the same region (Figure 5). This is a direct evidence that the reason for the dominant radiation impact on GPP_{IAV} in the very-wet pixels is due to its high sensitivity to radiation, not high radiation anomaly (Figure 5). In the driest tropical pixels (very-dry to

semi-dry pixels), the IAV of GPP, ER, and NEE are dominated by precipitation, which is due to the extremely high sensitivity not due to the magnitude of precipitation anomalies, since the precipitation anomalies in those regions are the weakest.

The shifting of relative contributions of climate drivers to C flux IAV in time, —such as between dry and wet seasons or El Niño and La Niña events— are also primarily driven by changes in the *sensitivities* of carbon flux to climate anomalies, rather than by the *magnitude* of climate anomalies. This is supported by the similar contrast of the sensitivity of C flux IAV to climate anomalies between dry and wet (Figure S15) and between El Niño vs. La Niña (Figure S16) with the observed shift in the relative influence of different climate factors to C flux IAV (Figure S13-14).

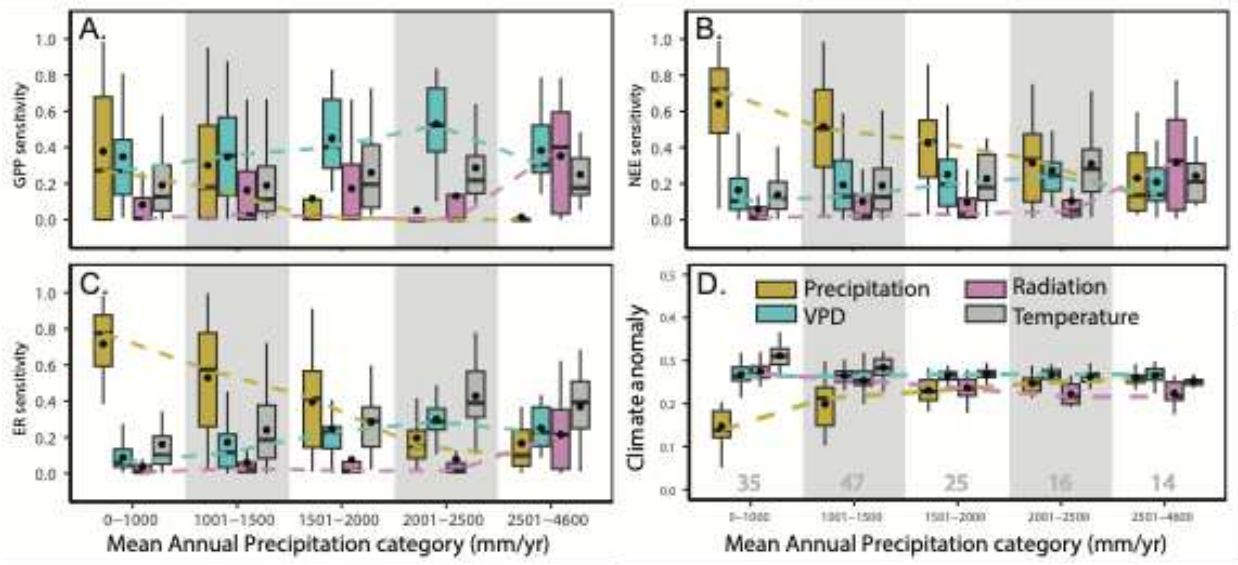


Figure 5. GPP, NEE, and ER relative sensitivities to climate IAV (A, B, C, unit=1) and standardized climate anomaly (D, unit=1) (Methods) during 2010-2021. Grid-cell data is grouped according to the MAP category. Boxes and whiskers show median, 5%, 25%, 75%, and 95% percentiles.

3. DISCUSSION

Tropical carbon flux variability is primarily driven by climatological limitations

Using data-constrained CARDAMOM model, we quantify the contributions of major climate drivers to the tropical land carbon flux IAV at grid-cell level. This approach substantially enhances the spatial and process

297 level understanding of climate controls on tropical carbon flux IAV. We find that the dominant climate
298 drivers for tropical carbon flux IAV differ among GPP, ER, and NEE, and that their relative contributions
299 strongly depend on local climate conditions, especially mean precipitation. Along a gradient from very wet
300 to very dry climates, the contributions of temperature, radiation, and VPD systematically decrease, while
301 the contribution of precipitation increases. In the dry and very dry regions, precipitation accounts for more
302 than 40% of the IAV in GPP, ER, and NEE, whereas in very wet regions its contribution declines to ~0–
303 20%. In contrast, radiation contributes up to ~20% of the IAV in ER and NEE and ~40% in GPP under very
304 wet conditions. This strong dependence of climate contributions on local hydroclimate also applies in time:
305 the contributions of precipitation are much larger during dry season and dry climate events (e.g., El Niña)
306 than during wet season and wet climate events (e.g., La Nina).

307 This diverse dominant climate drivers for tropical carbon flux IAV is consistent with previous studies that
308 investigate dominant climate drivers for a particular vegetation type or a region. For example, the finding
309 that radiation dominates GPP_{IAV} and NEE_{IAV} in the moist tropical forests, including northwest Amazon and
310 western Congo forest, (Figure 1A) is consistent with previous studies showing that the wetter part of the
311 Amazon rainforest is photosynthetically light limited, due to frequent cloud covering that reduces light
312 availability [10,11,14].

313 In the seasonally moist rainforests (MAP<2800mm), VPD, instead of radiation, dominates GPP_{IAV} (Figure
314 1-2), which is consistent with results based on SIF[24]. The average precipitation of seasonally moist
315 rainforest is 1740mm in the Congo rainforest and 2342mm in the Amazon, much lower than the moist
316 Amazon rainforest (3024mm), during our investigated period (2010-2021, ERA5 data, Figure 2). Thus, the
317 seasonally moist forest are more vulnerable to hydraulic damage when VPD is high [25–29]. The seasonally
318 moist rainforest has higher VPD_{IAV} compared to the moist rainforest. Increasing VPD causes plants to close
319 their stomata to minimize water loss, at a cost of hydraulic stress and less substrate for dark reactions in
320 photosynthesis. As reduced stomatal conductance limits the uptake of carbon dioxide (CO_2), ultimately
321 constraining carbon fixation and energy production and a reduction in GPP. High VPD under warm

322 temperatures can even lead to hydraulic damage, which can reduce the leaf biomass and the efficiency of
323 photosynthesis [30–33].

324 In tropical semiarid and grassland/cropland regions, where the annual precipitation is below a threshold of
325 1400mm, GPP_{IAV} is driven by precipitation year-to-year fluctuation. This finding is consistent with Jung et
326 al.[34] where they find water availability is the most important factor controlling the local IAV of GPP in
327 tropical semiarid and grassland/cropland regions. Satellite-based SIF also indicates that semiarid region
328 GPP fluctuations are mostly controlled by precipitation[35]. It is widely acknowledged that vegetation
329 productivity is primarily controlled by soil moisture limitation in low-rainfall areas [36,37].

330 The main focus of our study is to discuss the dominant climate factors for net ecosystem uptake of carbon
331 (NEE), instead of the net biosphere C exchange (NBE), which include fire. We looked at the relative
332 importance of fire on carbon fluxes IAV. We find that fire is less important than any other climate factor,
333 including the interaction effects (Figure S17), in most regions, except its contribution to NBE_{IAV} in the very
334 dry regions. Additionally, local geography and nutrients availability may also drive heterogenous
335 ecosystem response to climate anomalies[38], which is beyond the scope of this study.

336

337 **Dominant climate factor for NEE_{IAV} mirrors ER_{IAV}, instead of GPP_{IAV}**

338 Dominant climate factor for NEE_{IAV} is the net outcome of GPP_{IAV} and ER_{IAV}. Although the distribution of
339 climate factors for NEE_{IAV} and ER_{IAV} follows a similar pattern as GPP_{IAV}, where it shows some impact
340 from radiation for both NEE and ER in the moist rainforests and VPD for the seasonally moist rainforests
341 (Figure 1), the dominant climate factor for NEE_{IAV} more closely mirrors ER than GPP. Aggregating pixel
342 level dominant drivers to latitudinal mean / biogeographic regions, both NEE_{IAV} and ER_{IAV} are dominated
343 by precipitation across almost all climate categories (Figure 2), which is consistent with a study that found
344 water availability drives NEE_{IAV} and ER_{IAV}[17].

Ecosystem respiration includes its aboveground (autotrophic respiration, Ra) and belowground (Ra from root and heterotrophic respiration from soil microbes, Rh) components (Figure S8). The dominant climate factor for Ra is almost the same as GPP, while the dominant climate factor for Rh is precipitation (Figure S8). Rh is a major component of soil respiration. A machine-learning based data-driven global soil heterotrophic respiration dataset reveals that precipitation is the dominant climate factor for soil respiration over all the regions except tropics , supporting the results from our study[39].

Over dry and semi-dry regions (1001-2000mm/yr) (Figure 2), the mirroring of NEE_{IAV} of ER_{IAV} reflects the larger sensitivity of ER_{IAV} to precipitation than GPP. For example, in the tropical African dry region, although both GPP_{IAV} and ER_{IAV} are dominated by precipitation over most points (Figures 1 and 2), ER has much higher sensitivity to precipitation (Figure 1). ER also shows a sudden drop when drought starts and an instant, dramatic rise when soil rewets, a phenomenon called "birch effect" [40–42], which causes the large contributions of ER_{IAV} to NEE_{IAV} and the dominant role of precipitation to NEE_{IAV}.

In the tropical wet and very-wet regions (above 2001mm/yr), the dominant climate factor influencing NEE_{IAV} is the same as its Rh component. In these regions, the contributions of temperature, radiation, and VPD to GPP_{IAV} and ER_{IAV} becomes substantially larger than in drier regions. Temperature even becomes the largest contributor to ER_{IAV} in the very-wet region instead of precipitation in other regions, a result consistent with[39]. In contrast, the contribution of precipitation to GPP_{IAV} is close to zero, whereas precipitation still contributes more than 20% to ER_{IAV} (Figure 2). In these very wet regions, increase in radiation are typically accompanied by increases in temperature which together enhance photosynthesis and autotrophic respiration through greater light availability and higher biochemical and metabolic rates[24]. At the same time, warmer-than-average conditions could promote microbial decomposition and heterotrophic respiration. Thus, increase of GPP under warmer conditions partially offsets by increase of ER, leading to a much smaller impact of temperature and radiation on NEE_{IAV}. By contrast, precipitation primarily affects ER through soil moisture constraint on heterotrophic respiration; therefore, its influence becomes more important than other climate factors for NEE_{IAV} in these wet regions.

Limitation

CARDAMOM's mechanistic framework, combined with its ability to assimilate diverse observational constraints, represents a substantial advance for quantifying ecosystem processes beyond what can be inferred from individual satellite-derived products alone. Nevertheless, several limitations of the framework and important caveats associated with the assimilated data streams must be acknowledged.

First, as with any data assimilation system, model–data agreement is strongly dependent on the assumed error statistics of the assimilated observations. Smaller prescribed uncertainties generally lead to closer agreement between model outputs and the corresponding datasets. As shown in Figures S1–S3, CARDAMOM achieves better fits to assimilated GPP and aboveground biomass (AGB) than to net biome exchange (NBE) anomalies and terrestrial water storage (TWS). This difference likely reflects the longer temporal coverage and relatively smaller assumed uncertainties associated with the GPP and AGB datasets. Sensitivity tests indicate that reducing the assumed uncertainties in NBE and TWS improves agreement with these datasets but degrades the fit to GPP and AGB, suggesting potential inconsistencies among the assimilated products and/or missing or incomplete process representations within CARDAMOM. Addressing these issues will require future efforts to better characterize observational uncertainties, harmonize multi-source datasets, and further refine key ecosystem process representations within the model.

Second, several assimilated data products are themselves model-derived and constrained by observations, rather than being direct measurements. For example, the GPP product used here is generated by a machine-learning framework trained on flux tower observations and satellite data. The sparse spatial coverage of flux towers in tropical regions may therefore introduce additional uncertainty and potential biases in GPP estimates over the tropics. Expanding independent observational networks and developing improved

evaluation strategies in data-poor regions remain critical for strengthening the reliability of assimilated products and, ultimately, for advancing our understanding of the tropical carbon cycle.

Implication

Our study goes beyond quantifying the relative contributions of climate drivers to tropical carbon flux IAV but also reveals that this shifting of dominant climate drivers is closely correlated with local water availability, which applies in both space and time. These findings provide a possible mechanistic explanation for the observed changes in the sensitivity of atmospheric CO_2 growth rate to climate anomalies in recent decades. It also implies that the carbon-climate sensitivity will likely change with the changes of climate. These results further suggest that precipitation will play an increasingly important role in carbon-flux IAV in tropical South America under the projected drying, while VPD and radiation are likely to become more influential across parts of Africa under projected wetting. Our results highlight that accurately representing the dependence of carbon-climate sensitivity on local hydroclimate will be critical to predict changes of future tropical carbon cycle.

METHODS

We use a process-based model (DALEC) embedded in a data-model integration system (CARbon Data Model fraMework, CARDAMOM) and a suite of satellite constraints to investigate temperature, precipitation, vapor pressure deficit (VPD), and radiation interannual variability (IAV) on the IAV of gross primary productivity (GPP), ecosystem respiration (ER), and net ecosystem exchange (NEE) at local and regional scales. In the following, we describe the model structure, forcings, observational constraints, the Bayesian Model-data fusion framework, climate perturbation methods, and the use of the data-constrained DALEC model to determine the dominant climatic drivers of the tropical carbon IAV.

CARDAMOM model-data fusion system and DALEC-JCR model structure

CARDAMOM is a model-data fusion (MDF) system that constrains model parameters and initial states in a process-oriented model - the Data Assimilation Linked Ecosystem Carbon model (DALEC, Figure S18) - and a Bayesian model-data integration algorithm using adaptive Metropolis algorithm[43]. In contrast to more complex process-based terrestrial biosphere models, the relatively parsimonious DALEC C cycle model structures allow for joint optimization of highly uncertain process parameters (such as initial carbon and water states, photosynthetic parameters, C allocation, turnover rates, and their dependencies on soil moisture) based on the available observations of carbon and water variables[44–50]. While typically incorporation of complexity in models is beneficial for process representation, Famiglietti et al.[44] show that model complexity advantages are fundamentally limited when insufficient data is available to support parameter inference. The DALEC model-embedded CARDAMOM MDF system has been applied to a range of spatial scales with a suite of eddy covariance and satellite datasets to (i) represent C cycles, (ii) optimize critical parameters and states, and (iii) infer C cycle-associated climate sensitivities[44–50].

Here we briefly introduce how CO_2 fluxes are simulated and scaled by environmental drivers in the DALEC model, which is most relevant to this study. Complete descriptions of model structure can be found in Bloom et al.[51]. GPP is calculated based on the biochemistry of C3 and C4 photosynthesis to determine potential leaf-level photosynthesis, which is calculated in terms of two potentially limiting rates: Rubisco limited rate and light-limited rate. Moisture stress factor is related to the mean soil moisture concentration in the root zone and affects the light-limited rate. The stomatal conductance is calculated using the Medlyn stomatal conductance model[52]. DALEC represents water stress constraints on GPP and stomatal conductance based on water potential along the soil-plant continuum. Autotrophic respiration is calculated as a proportional flux to GPP. Transpiration is computed using the Penman–Monteith equation. Heterotrophic CO_2 is respired both anaerobically and aerobically, both as a function of C turnover rate, soil temperature, soil moisture, and the volumetric fraction of aerobic/anaerobic soil.

Following Bloom & Williams[45], we provide 4º (latitude) x 5º (longitude) resolution, monthly meteorological forcing dataset for DALEC (namely monthly temperature, total precipitation, snowfall,

441 global incident shortwave radiation, vapor pressure deficit, CO_2, and burned area) obtained from the
442 European Centre for Medium-Range Weather Forecasts (ECMWF) Reanalysis v5 (ERA5) [53] to drive
443 DALEC model at each grid-cell. Satellite observations we use to constrain the model are listed in Table 1.

444 **Table 1 Observation datasets used in data-model fusion**

Observations (abbreviation)	Observation data sources	Number of observational constraints	Frequency
Leaf area index (LAI)	[1]MODIS LAI retrievals [54]	1	Climatology
Soil organic carbon (SOC)	HWSD for initial SOC [55]	1	Climatology
Above- and Below- ground biomass (ABGB)	Annual 2001-2020 ABGB [56]	20	Annual
Solar-induced fluorescence (SIF)	[2]Monthly part 2018-2021 TROPOMI retrievals of SIF[57]		Monthly
Fire C emissions (BB)	Mean 2001-2015 4° x 5° inverse estimates of fire C emissions [58]	1	Climatology
Net biospheric exchange (NBE)	[3]Monthly 2010-2018 4° x 5° inverse estimates of terrestrial NBE CMS-FLUX NBE 2020[59]	108	Monthly
Total water storage anomaly (TWS)	Monthly 2002-2017, 2018-2021 GRACE/GRACE-FO retrieval of terrestrial water storage anomaly [60]	237	Monthly
Gross primary production (GPP)	Monthly 2001-July2020 FluxSat GPP v2 Based on MODIS and FLUXNET[61]	235	Monthly

445 [1]Only mean 2001-2021 LAI is assimilated into CARDAMOM, to minimize the influence of seasonal LAI
446 retrieval biases[62]. [2]time-resolved SIF is assimilated as a relative constraint on the temporal variability of
447 GPP (Section 2.4 in Bloom et al lagged effect). [3]annual means and monthly variabilities of observed NBE
448 are used to constrain model (Section 2.4 in Bloom et al lagged effect).

449 **Bayesian Model-data fusion framework**

450 The initial states and parameters of DALEC-JCR are constrained in a Bayesian optimization framework
451 (CARbon Data Model fraMework, CARDAMOM). The CARDAMOM framework uses Bayes' theorem to

optimize the posterior probability of initial states and time-invariant process parameters ($\boldsymbol{y}$), given observations $\boldsymbol{O}$, p($\boldsymbol{y}|\boldsymbol{O}$), as follows:

$$p(\boldsymbol{y}|\boldsymbol{O}) \propto p(\boldsymbol{y})p(\boldsymbol{O}|\boldsymbol{y}) \quad (1)$$

where p($\boldsymbol{y}$) is the prior probability distribution of $\boldsymbol{y}$, and p($\boldsymbol{O}|\boldsymbol{y}$) is proportional to the likelihood of $\boldsymbol{y}$ given $\boldsymbol{O}$, L($\boldsymbol{y}|\boldsymbol{O}$). Assuming errors are uncorrelated, the overall likelihood of $\boldsymbol{y}$ given $\boldsymbol{O}$ can be expressed as:

$$L(y|O) = L_{NEE}\, L_{GPP} L_{SIF} L_{ABGB} L_{EWT} L_{CO} \quad (2)$$

We derive the corresponding likelihood function L_* (i.e., L_{NEE}) as follows:

$$L_* = e^{-\frac{1}{2}\sum_i} \left(\frac{m_i(y)-o_i}{\sigma_i}\right)^2 \quad (3)$$

where o_i and $m_i(\mathbf{y})$ correspond to the i^{th} observation and the corresponding modeled quantity derived from control vector $\mathbf{y}$, respectively; σ_i accounts for the combined errors from the DALEC model structure, forcing drivers, and observations. Following [21], we retrieve the distribution of p($\mathbf{y}$|O) at each grid-cell by running four adaptive Metropolis-Hastings Markov Chain Monte Carlo chains for 10^8 iterations.

Climate perturbations

Perturbation method

To characterize the relative impact of climate driver variability on tropical caron IAV, we designed five climate perturbation scenarios, listed in Table S1. We denote the modeled C fluxes, $\boldsymbol{C}$, as a function of time-dependent meteorological drivers ($\boldsymbol{M}$) and time-invariant model parameters and initial states ($\boldsymbol{y}$):

$$\boldsymbol{C} = \text{DALEC}(\boldsymbol{M},\boldsymbol{y}) \quad (4)$$

where $\boldsymbol{C}$ represents carbon fluxes or carbon pools. The *DALEC* operator denotes the DALEC model simulation driven by forcing $\boldsymbol{M}$ and parameters $\boldsymbol{y}$. Model simulation scenarios: control model run ($\boldsymbol{M}_{ori}$) use ERA5 reanalysis data. Perturbed model runs: replace climate drivers with 2010-2021 climatology ($\boldsymbol{M}_{pert}$),

including four single-factor perturbations (P, T, R, and V are short for precipitation, temperature, radiation, and VPD), and one full-factor perturbation (PTRV). Although the model is run from 2001 to 2021 for validation, we use 2010-2021 for our climate perturbation analysis due to a stronger constraint from observations as NBE from CMS Flux starts in 2010.

We take two steps to evaluate the relative importance of climate drivers' variability to tropical caron IAV:

STEP 1: Calculate the mean monthly climatology of precipitation, temperature, radiation, and VPD. We then replace the original drivers with climatology mean in five scenarios.

STEP 2: We then calculate the difference of carbon fluxes/pool between original and perturbed climates:

$$dC_M = C_{ori} - C_{pert} \quad (5)$$

where ***M*** could be any single perturbation scenario: P, T, R, V, or the full climate factors perturbation scenario: PTRV. By definition, we can derive the interactive effect of climate factors on carbon fluxes (***dCi***) using Eqn 6:

$$dCptrv = dCi + dCt + dCp + dCr + dCv \quad (6)$$

We use the carbon response index **K** to represent the anomaly of carbon responses to climate variables:

$$\mathbf{K_M} = \text{time series mean}(|dC_M|) \quad (7)$$

To evaluate the relative importance of the interaction effect as well as each single climate factor to the change of carbon fluxes/states, we use eqn (8):

$$K_{dCM}/(K_{dCt} + K_{dCp} + K_{dCr} + K_{dCv} + K_{dCi}) \quad (8)$$

Note that because we took the absolute value of dC at each time step, $(K_{dCt} + K_{dCp} + K_{dCr} + K_{dCv} + K_{dCi}) / K_{dCptrv}$ does not equal one, $K_{dCm}$is different from dC_m.

Carbon flux sensitivities to climate change

To answer whether it is the magnitude of climate IAV, or the flux sensitivity to the climate anomaly, that led to heterogeneous dominant climate factors for carbon fluxes in different tropical ecosystems, we use climate anomaly standardized by the mean value to represent the magnitude of climate IAV (met_{ano}, Figure 5D). We then calculate carbon fluxes sensitivity to climate change by dividing carbon response $\boldsymbol{dC_M}$ with time series mean of normalized climate anomaly. Normalization was done by dividing the climate anomaly with the average magnitude of climate anomalies. Purpose of our normalization is to make flux sensitivities to climate drivers inter-comparable, by bringing the magnitudes each climate driver on the same scale.

Data and code availability:

Data and code for generating figures are available at [63].

References

1. Cox, P. M. *et al.* Sensitivity of tropical carbon to climate change constrained by carbon dioxide variability. *Nature* **494**, 341–344 (2013).
2. Anderegg, W. R. L. *et al.* Tree mortality from drought, insects, and their interactions in a changing climate. *New Phytologist* **208**, 674–683 (2015).
3. Kindermann, J., Würth, G., Kohlmaier, G. H. & Badeck, F. Interannual variation of carbon exchange fluxes in terrestrial ecosystems. *Global Biogeochemical Cycles* **10**, 737–755 (1996).
4. Wang, W. *et al.* Variations in atmospheric CO_2 growth rates coupled with tropical temperature. *Proc. Natl. Acad. Sci. U.S.A.* **110**, 13061–13066 (2013).
5. Wang, X. *et al.* A two-fold increase of carbon cycle sensitivity to tropical temperature variations. *Nature* **506**, 212–215 (2014).
6. Humphrey, V. *et al.* Sensitivity of atmospheric CO2 growth rate to observed changes in terrestrial water storage. *Nature* **560**, 628–631 (2018).

7. Liu, L. *et al.* Increasingly negative tropical water-interannual CO2 growth rate coupling. *Nature* **618**, 755–760 (2023).
8. Wang, X. *et al.* A two-fold increase of carbon cycle sensitivity to tropical temperature variations. *Nature* **506**, 212–215 (2014).
9. Liu, L. *et al.* Increasingly negative tropical water–interannual CO2 growth rate coupling. *Nature* **618**, 755–760 (2023).
10. Saleska, S. R., Didan, K., Huete, A. R. & Da Rocha, H. R. Amazon Forests Green-Up During 2005 Drought. *Science* **318**, 612–612 (2007).
11. Huete, A. R. *et al.* Amazon rainforests green-up with sunlight in dry season. *Geophysical Research Letters* **33**, 2005GL025583 (2006).
12. Wang, Y. *et al.* Elucidating climatic drivers of photosynthesis by tropical forests. *Global Change Biology* **29**, 4811–4825 (2023).
13. Braghiere, R. K. *et al.* Characterization of the radiative impact of aerosols on CO_2 and energy fluxes in the Amazon deforestation arch using artificial neural networks. *Atmos. Chem. Phys.* **20**, 3439–3458 (2020).
14. Nemani, R. R. *et al.* Climate-Driven Increases in Global Terrestrial Net Primary Production from 1982 to 1999. *Science* **300**, 1560–1563 (2003).
15. Poulter, B. *et al.* Contribution of semi-arid ecosystems to interannual variability of the global carbon cycle. *Nature* **509**, 600–603 (2014).
16. Ahlström, A. *et al.* The dominant role of semi-arid ecosystems in the trend and variability of the land CO_2 sink. *Science* **348**, 895–899 (2015).
17. Jung, M. *et al.* Compensatory water effects link yearly global land CO2 sink changes to temperature. *Nature* **541**, 516–520 (2017).

18. Barkhordarian, A., Saatchi, S. S., Behrangi, A., Loikith, P. C. & Mechoso, C. R. A Recent Systematic Increase in Vapor Pressure Deficit over Tropical South America. *Sci Rep* **9**, 15331 (2019).
19. Fu, R. *et al.* Increased dry-season length over southern Amazonia in recent decades and its implication for future climate projection. *Proc. Natl. Acad. Sci. U.S.A.* **110**, 18110–18115 (2013).
20. Gebrechorkos, S. H. *et al.* Warming accelerates global drought severity. *Nature* **642**, 628–635 (2025).
21. Bloom, A. A. *et al.* Lagged effects regulate the inter-annual variability of the tropical carbon balance. *Biogeosciences* **17**, 6393–6422 (2020).
22. Sun, W. *et al.* Biome-scale temperature sensitivity of ecosystem respiration revealed by atmospheric CO2 observations. *Nat Ecol Evol* **7**, 1199–1210 (2023).
23. Green, J. K., Berry, J., Ciais, P., Zhang, Y. & Gentine, P. Amazon rainforest photosynthesis increases in response to atmospheric dryness. *Sci. Adv.* **6**, eabb7232 (2020).
24. Wang, Y. *et al.* Elucidating climatic drivers of photosynthesis by tropical forests. *Global Change Biology* **29**, 4811–4825 (2023).
25. Blackman, C. J. *et al.* Drought response strategies and hydraulic traits contribute to mechanistic understanding of plant dry-down to hydraulic failure. *Tree Physiology* **39**, 910–924 (2019).
26. Brodribb, T. J. & Cochard, H. Hydraulic Failure Defines the Recovery and Point of Death in Water-Stressed Conifers. *Plant Physiology* **149**, 575–584 (2009).
27. Johnson, D. M., Katul, G. & Domec, J. Catastrophic hydraulic failure and tipping points in plants. *Plant Cell & Environment* **45**, 2231–2266 (2022).

28. McDowell, N. G. Mechanisms Linking Drought, Hydraulics, Carbon Metabolism, and Vegetation Mortality. *Plant Physiology* **155**, 1051–1059 (2011).
29. Li, M.-Y. *et al.* Greater risk of hydraulic failure due to increased drought threatens pine plantations in Horqin Sandy Land of northern China. *Forest Ecology and Management* **461**, 117980 (2020).
30. Gentine, P. *et al.* Coupling between the terrestrial carbon and water cycles—a review. *Environ. Res. Lett.* **14**, 083003 (2019).
31. Grossiord, C. *et al.* Plant responses to rising vapor pressure deficit. *New Phytologist* **226**, 1550–1566 (2020).
32. Massmann, A., Gentine, P. & Lin, C. When Does Vapor Pressure Deficit Drive or Reduce Evapotranspiration? *J Adv Model Earth Syst* **11**, 3305–3320 (2019).
33. Schönbeck, L. C. *et al.* Increasing temperature and vapour pressure deficit lead to hydraulic damages in the absence of soil drought. *Plant Cell & Environment* **45**, 3275–3289 (2022).
34. Jung, M. *et al.* Compensatory water effects link yearly global land CO2 sink changes to temperature. *Nature* **541**, 516–520 (2017).
35. Zhang, Y. *et al.* Precipitation and carbon-water coupling jointly control the interannual variability of global land gross primary production. *Sci Rep* **6**, 39748 (2016).
36. Dubey, N. & Ghosh, S. The relative role of soil moisture and vapor pressure deficit in affecting the Indian vegetation productivity. *Environ. Res. Lett.* **18**, 064012 (2023).
37. Krueger, E. S. *et al.* Grassland productivity estimates informed by soil moisture measurements: Statistical and mechanistic approaches. *Agronomy Journal* **113**, 3498–3517 (2021).

38. Hofhansl, F. *et al.* Sensitivity of tropical forest aboveground productivity to climate anomalies in SW Costa Rica. *Global Biogeochemical Cycles* **28**, 1437–1454 (2014).
39. Yao, Y. *et al.* A Data-Driven Global Soil Heterotrophic Respiration Dataset and the Drivers of Its Inter-Annual Variability. *Global Biogeochemical Cycles* **35**, e2020GB006918 (2021).
40. Metz, E.-M. *et al.* Soil respiration–driven CO_2 pulses dominate Australia's flux variability. *Science* **379**, 1332–1335 (2023).
41. Metz, E.-M., Vardag, S. N., Basu, S., Jung, M. & Butz, A. Seasonal and interannual variability in CO_2 fluxes in southern Africa seen by GOSAT. *Biogeosciences* **22**, 555–584 (2025).
42. Yun, J. *et al.* Interannual Variability in African Regional Ecosystem Carbon Fluxes and Their Drivers Revealed by Satellite Observations. *Global Biogeochemical Cycles* **39**, e2025GB008597 (2025).
43. Haario, H., Saksman, E. & Tamminen, J. An Adaptive Metropolis Algorithm. *Bernoulli* **7**, 223 (2001).
44. Famiglietti, C. A. *et al.* Optimal model complexity for terrestrial carbon cycle prediction. *Biogeosciences* **18**, 2727–2754 (2021).
45. Bloom, A. A. & Williams, M. Constraining ecosystem carbon dynamics in a data-limited world: integrating ecological 'common sense' in a model–data fusion framework. *Biogeosciences* **12**, 1299–1315 (2015).
46. Quetin, G. R., Bloom, A. A., Bowman, K. W. & Konings, A. G. Carbon Flux Variability From a Relatively Simple Ecosystem Model With Assimilated Data Is Consistent With Terrestrial Biosphere Model Estimates. *J Adv Model Earth Syst* **12**, e2019MS001889 (2020).

47. Williams, M., Schwarz, P. A., Law, B. E., Irvine, J. & Kurpius, M. R. An improved analysis of forest carbon dynamics using data assimilation. *Global Change Biology* **11**, 89–105 (2005).
48. Yeager, S. G. *et al.* The Seasonal-to-Multiyear Large Ensemble (SMYLE) prediction system using the Community Earth System Model version 2. *Geosci. Model Dev.* **15**, 6451–6493 (2022).
49. Ma, S. *et al.* Resolving the Carbon-Climate Feedback Potential of Wetland CO_2 and CH_4 Fluxes in Alaska. *Global Biogeochemical Cycles* **37**, e2022GB007524 (2023).
50. Norton, A. J. *et al.* Improved process representation of leaf phenology significantly shifts climate sensitivity of ecosystem carbon balance. *Biogeosciences* **20**, 2455–2484 (2023).
51. Bloom, A. A. *et al.* Lagged effects regulate the inter-annual variability of the tropical carbon balance. *Biogeosciences* **17**, 6393–6422 (2020).
52. Medlyn, B. E. *et al.* Reconciling the optimal and empirical approaches to modelling stomatal conductance. *Global Change Biology* **18**, 3476–3476 (2012).
53. Berrisford, P. *et al. The ERA-Interim Archive Version 2.0*. *ERA Report Series* (ECMWF, Shinfield Park, Reading, 2011).
54. Myneni, R., Knyazikhin, Y. & Park, T. MOD15A2H MODIS/Terra Leaf Area Index/FPAR 8-Day L4 Global 500m SIN Grid V006. NASA Land Processes Distributed Active Archive Center https://doi.org/10.5067/MODIS/MOD15A2H.006 (2015).
55. European Commission. Joint Research Centre. Institute for Environment and Sustainability. *Global Soil Organic Carbon Estimates and the Harmonized World Soil Database*. (Publications Office, LU, 2011).

56. Xu, L. *et al.* Changes in global terrestrial live biomass over the 21st century. *Sci. Adv.* **7**, eabe9829 (2021).
57. Doughty, R. *et al.* TROPOMI reveals dry-season increase of solar-induced chlorophyll fluorescence in the Amazon forest. *Proc. Natl. Acad. Sci. U.S.A.* **116**, 22393–22398 (2019).
58. Bowman, K. W. *et al.* Global and Brazilian Carbon Response to El Niño Modoki 2011–2010. *Earth and Space Science* **4**, 637–660 (2017).
59. Liu, J. *et al.* Carbon Monitoring System Flux Net Biosphere Exchange 2020 (CMS-Flux NBE 2020). *Earth Syst. Sci. Data* **13**, 299–330 (2021).
60. TELLUS. JPL GRACE Mascon Ocean, Ice, and Hydrology Equivalent Water Height RL05M.1 CRI Filtered Version 2. NASA Physical Oceanography Distributed Active Archive Center https://doi.org/10.5067/TEMSC-2LCR5 (2016).
61. Joiner, J. & Yoshida, Y. Vegetation CollectionGlobal MODIS and FLUXNET-derived Daily Gross Primary Production, V2. 0 MB Preprint at https://doi.org/10.3334/ORNLDAAC/1835 (2021).
62. Bi, J. *et al.* Sunlight mediated seasonality in canopy structure and photosynthetic activity of Amazonian rainforests. *Environ. Res. Lett.* **10**, 064014 (2015).
63. Ma, S. From rain to radiance - Dominant drivers of tropical carbon flux interannual variability shift with local climate. Zenodo https://doi.org/10.5281/ZENODO.15225728 (2025).

Acknowledgment

Part of the research was carried out at the Jet Propulsion Laboratory, California Institute of Technology, under a contract with the National Aeronautics and Space Administration, (80NM0018D0004).

Funding
This research was supported by NASA Carbon Cycle Science Program with the funding number 80NM0018F0590.

Author contributions:

Conceptualization: J.L;A.A.B;S.M;D.S;
Methodology: J.L;A.A.B;S.M;
Investigation: J.L;A.A.B;S.M;L.P;R.D;A.N;
Visualization: J.L;A.A.B;S.M;R.B;E.B;
Supervision: J.L;A.A.B;S.M;
Writing—original draft: J.L;A.A.B;S.M;
Writing—review & editing: J.L;A.A.B;S.M;R.B;E.B;J.W;R.D;A.N;

Competing interests:
There is no competing interests.

Supplementary Files

This is a list of supplementary files associated with this preprint. Click to download.

- tropicalCIAVsupplement02May2026.pdf